ACS APPLIED POLYMER MATERIALS

pubs.acs.org/acsapm Article

Hot Air Permeable Preceramic Polymer Derived Reticulated Ceramic Foams

Tugce Semerci, Murilo Daniel de Mello Innocentini, Gabriel Antonio Marsola, Paulo Renato Orlandi Lasso, Gian Domenico Soraru, and Cekdar Vakifahmetoglu*

Cite This: ACS Appl. Polym. Mater. 2020, 2, 4118–4126 Read Online

ACCESS | Metrics & More | Article Recommendations | Supporting Information

ABSTRACT: Open and partially closed cell polymer derived ceramic, specifically silicon oxycarbide, foams were produced from commercially available polyurethane (PU) foams through the replica technique combined with the preceramic polymer pyrolysis route. The focus was directed on the role of PU morphology (cell size and open/partially closed cells), synthesis parameters (cross-linking temperature and time), and type of the polysiloxane precursors for fine-tuning the microstructural features of the resulting ceramic foams and their eventual effect on the fluid dynamic/mechanical properties. Consequently, ceramic foams having dense/hollow struts with/without hierarchical porosity were able to be manufactured and characterized in detail. The average total porosity including all compositions was above 95%, the maximum surface area was found to be reaching 79 $m^2.g^{-1}$, and the room temperature permeability measurements indicated a wide range for k_1 (0.28×10^{-9}–11.48×10^{-9} m^2) and k_2 (0.34×10^{-5}–54.17×10^{-5} m) according to the selected PU substrate. Hot air permeation tests showed that the foams were stable up to 700 °C without any loss of functionality. Accordingly, they are envisioned to be employed as reusable air filtration device parts for pollutants (viruses, bacteria, dust, etc.), catalytic supports, and filter components for reactions occurring in aggressive environments.

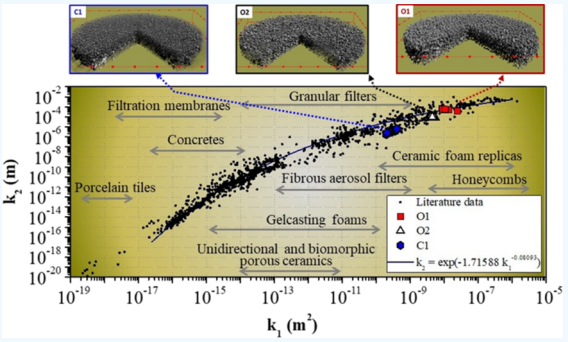

KEYWORDS: *foams, gas permeability, compression test, microtomography, polymer derived ceramics*

1. INTRODUCTION

Refractory porous ceramics are widely used in fluid flow and separation applications where the active components must withstand aggressive operational conditions, including chemical attack and high temperatures or pressures. Well-established examples include removal of slag and inclusions from molten metals, particulate filtration of hot gas streams, and thermocatalytic conversion of chemicals.[1−11] In these applications, a major operational cost is related to the power consumption of pumps, compressors, and blowers to force the permeation of liquids and gases through the porous ceramic matrix. There is a direct proportionality of the power consumption with the pressure drop resulting from the fluid flow, which in turn is influenced by the operational conditions and by the permeability of the porous structure. By the correct manipulation of pore characteristics, such as morphology, size, and fraction, pore topology and so the permeability coefficients of the medium can be optimized during the processing step to help the minimization of costs during the operation. However, since the porous structure also affects other important properties, such as mechanical strength, thermal conductivity, and so on, a balance is required to provide the best overall performance for the porous component.[12] It can be achieved by the suitable combination of ceramic formulation and the processing route used to fabricate the porous matrix.[13,14]

Silicon oxycarbide (SiOC) is an attractive ceramic material, produced via the Polymer Derived Ceramic (PDC) route, which can be used for producing cellular ceramic components, like reticulated ceramic foams, for demanding fluid flow applications. Due to its high-temperature stability, and chemical and oxidation resistances, porous PDCs can be used for thermal barriers, hot gas filtration, and catalyst supports.[1,15−22] It is known that such 3D interconnected foams enable improved catalytic activity via diffusion path reduction and a higher degree of reactant mixing.[23] It was previously shown that foams deliver more efficient heat transfer compared to particle beds and honeycombs. That is to say, foams offer better mass transfer/pressure drop trade-off with the advantage of radial mixing, and thus they are very suitable for applications such as gas filtration.[24,25]

Received: July 6, 2020
Accepted: August 19, 2020
Published: August 19, 2020

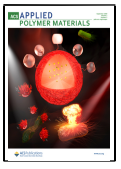

https://dx.doi.org/10.1021/acsapm.0c00734
ACS Appl. Polym. Mater. 2020, 2, 4118–4126

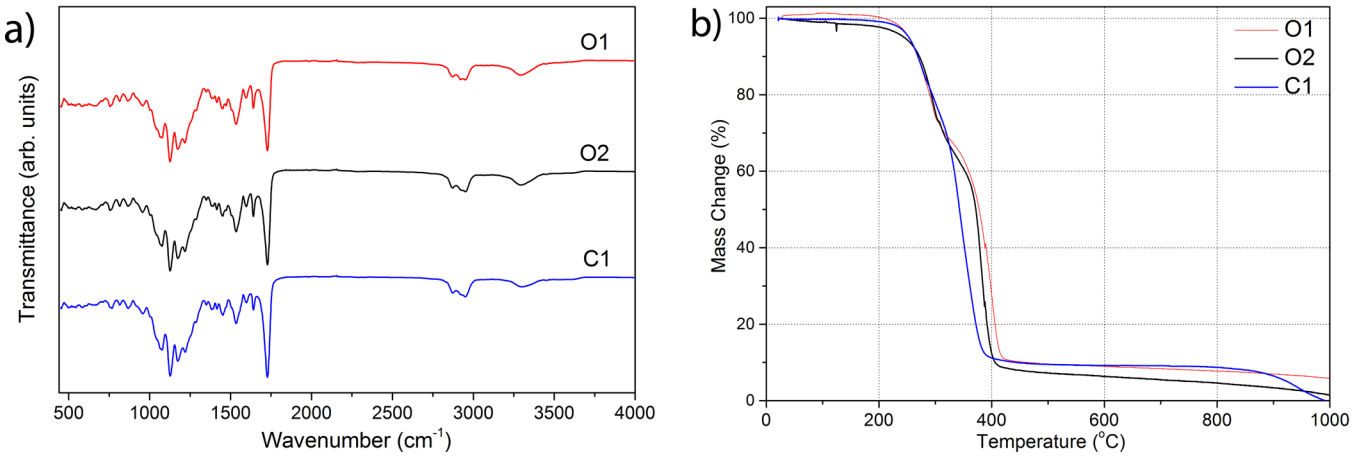

Figure 1. (a) FTIR spectra, and (b) TGA data of the O1, O2, and C1 PU foams (2 °C/min; N_2 flow 0.2 L/min).

Although PDC-based porous components can be obtained by following several different processing routes,[19,26,27] the replica technique is in fact the preferred one to form reticulated ceramic foams due to the simplicity of controlling the processing conditions.[28] One drawback of this route, however, is that the struts of these foams are generally hollow due to the template decomposition, causing a significant loss in the mechanical strength of the ceramic body. In a recent advance, macroporous PDC foams having not only hollow but also dense struts have been demonstrated by the replica technique.[29−33] Nevertheless, the processing conditions to obtain such reticulated ceramic foams with optimized properties have not yet been investigated in detail. Such skill provides an additional degree of freedom to engineer the pore structure depending on the end-user demands.

In the current work, the cross-linking conditions of the preceramic polymer blends were manipulated deliberately. This allowed the formation of ceramic foams having either hollow or dense struts, depending on the user request, formed by the so-called Schwartzwalder process, i.e., by the replica technique. Besides this, it was shown that polyurethane (PU) sponges with different pore connectivity (open and partially closed cells) could be used as templates to obtain diverse types of reticulated ceramic foams with different pore architectures. The aim of this study is to establish a strategy to manufacture macroporous PDC substrates with higher reproducibility which are more suitable for industrial applications. Moreover, the produced ceramic foams were also fully characterized with a focus in applications involving fluid permeation, aimed for the first time to correlate structural features of the foams with their permeability characteristics.

2. EXPERIMENTAL PROCEDURE

2.1. Materials. Polymer derived SiOC foams were produced using a mixture of polysiloxanes and three types of PU foams. Linear polyhydridomethylsiloxane (PHMS, MW ∼2100−2400, 30−45 cSt, CAS:63148-57-2, Gelest Inc., Morrisville, PA, USA) as the precursor, vinyl-terminated polydimethylsiloxane (PDMS, MW ∼62,700, 10,000 cSt, CAS:68083-19-2, Gelest Inc., Morrisville, PA, USA), and cyclic 2,4,6,8-tetramethyl-2,4,6,8-tetravinylcyclotetrasiloxane (TMTVS 97%, CAS:2554-06-5 Alfa Aesar, Ward Hill, MA, USA) were used as the cross-linking agents. For the curing process, 2.1−2.4% Pt platinum−divinyltetramethyldisiloxane complex in xylene (CAS: 68478-92-2, abcr GmbH, Kalsruhe, Germany) was diluted to 0.05% Pt in xylene and used. As templates, three different types of PU foams were used: two with open pores (sample O1 with 65 ppi (pores per inch), pore size 390 ± 93 μm, bulk density 0.029 ± 0.001 g/cm^3 and O2 with 80 ppi, pore size 316 ± 75 μm, bulk density 0.030 ± 0.002 g/cm^3), and one with partially closed pores (C1 with 59 ppi, pore size 429 ± 66 μm, bulk density 0.057 ± 0.002 g/cm^3, ARE S.r.l., Milan, Italy).

2.2. Replica Process. Three different preceramic polymer blends were prepared from PU/PHMS/PDMS/TMTVS (in weight ratio): (I) 1/2/0/0.08 (sample with no PDMS), (II) 1/1.7/0.3/0.08 (sample with 15% PDMS relative to PHMS), and (III) 1/1/1/0.08 (sample with 50% PDMS relative to PHMS). The samples with PDMS were formed since it is known that such polymer can be used to enhance the specific surface area (SSA) of the components by creating hierarchical porosity.[34] First, preceramic polymers (PHMS, PDMS, and TMTVS) were dissolved in acetone while stirring at 250 rpm at room temperature (RT) for 3 min. After homogenization, Pt catalyst (400 ppm relative to PHMS) was added dropwise and the mixture was stirred for 1 min at 200 rpm at RT. The blends were then transferred into separate Petri dishes where PU foams (diameter of ∼60 mm and thickness of ∼5 mm) were soaked and squeezed several times to remove the excess mixtures and this process was followed until the whole preceramic solutions were impregnated. The curing procedure was conducted under two different conditions to alter the final strut structure: (a) to yield dense struts: 80 °C for 7 h followed by RT curing for 23 h, and (b) to yield hollow struts: 220 °C for 2 h. All the cured foams were pyrolyzed under argon flow (200 mL/min) with a heating rate of 2 °C/min to 1000 °C and 2 h (dwell time) in an alumina tube furnace (PROTERM PTF 16/75/450, Ankara, Turkey).

2.3. Structural Characterizations. The microstructural features of the samples (fracture surfaces) were analyzed by scanning electron microscope (SEM, FEI Quanta 250 FEG, Hillsboro, OR, USA) after surface coating with ∼10 nm Au (Emitech K550X sputter coater, Quorum Technologies, UK). SEM images were subsequently analyzed using the ImageJ software (ImageJ 1.52a, National Institutes of Health, USA) to quantify the strut or cell size and distribution. In order to obtain the effective cell dimension, the average data (from 100 measurements) obtained by image analysis were converted to 3D values by applying the stereological equation: $D_{sphere} = D_{circle}/0.785$.[35] High-resolution X-ray micro-CT system (SkyScan, model 1172, Aartselaar, Belgium) was used to determine morphological parameters of SiOC foams. For each cylindrical sample, about 320 radial slice images (pixel size of 13.5 μm) were reconstructed to 8-bit BMP files (2000 × 2000 pixels) and analyzed as 3D images using the Brucker SkyScan software package (CTVOX, CTAN, CTVOL, and Dataviewer).

The thermal behavior of PU foams was studied under the same pyrolysis conditions by thermal gravimetric analysis (TGA, Shimadzu TGA-51, Shimadzu Corp., Japan). Samples were also analyzed by Fourier Transform Infrared Spectroscopy with attenuated total reflectance (FTIR-ATR, Spectrum Two with UATR fitted, Perkin Elmer, USA), wavenumber from 450 to 4000 cm^{-1}, 20 scans for each sample with 4 cm^{-1} resolution. The structural nature of SiOC foams

https://dx.doi.org/10.1021/acsapm.0c00734
ACS Appl. Polym. Mater. 2020, 2, 4118−4126

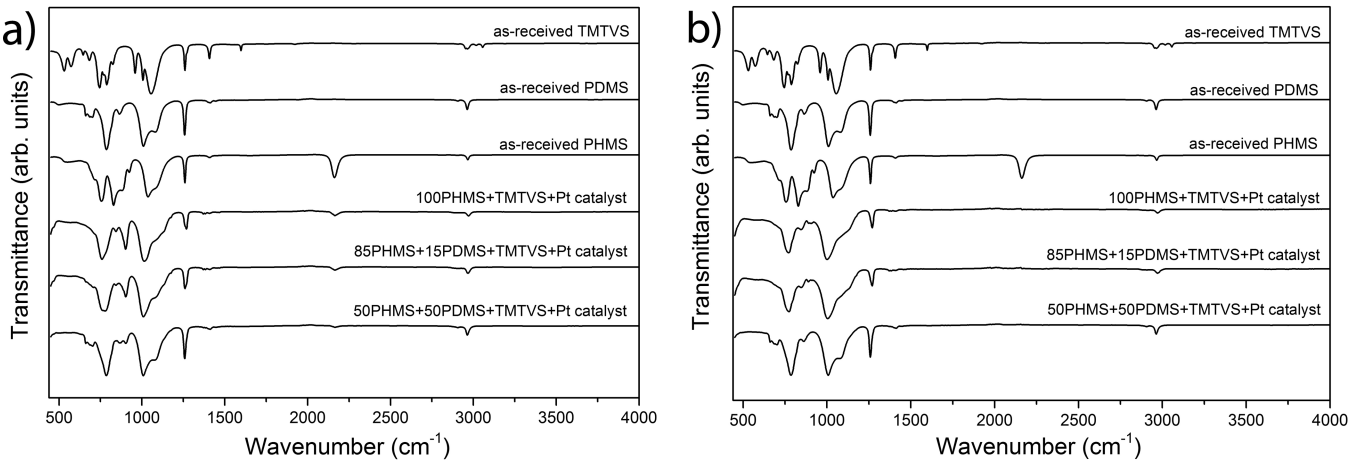

Figure 2. FTIR spectra of the as-received TMTVS, PDMS, PHMS, and preceramic precursors cross-linked at: (a) 80 °C/7 h + RT/23 h; (b) 220 °C/2 h.

was analyzed by X-ray diffraction (XRD, Philips X'Pert Pro) with CuKα radiation, step counting time of 3 s, and scan of 0.05°, between 10 and 90°.

The skeletal density (ρ_s) of powdered SiOCs fired samples was determined by a helium pycnometer (AccuPyc 1330, Micromeritics, Norcross, GA, USA). The bulk density (ρ_b) of SiOC foam samples was determined by relating their size and mass measurements, and total porosity (ε) was then calculated using both density values. N_2 sorption tests were done by Gemini V (Micromeritics, Norcross, GA, USA). The cold crushing strength (CCS) data were acquired by a TA.XT plus Texture Analyzer (Stable Micro System Ltd., Godalming, Surrey, UK) with a cross-head speed of 0.5 mm/s. Each data set was obtained from 10 samples with a cubic shape (~5 × 5 × 5 mm^3), and the measurements were continued until the first collapse.

2.4. Fluid Dynamic Characteristics. The produced ceramic foams were characterized first concerning their room temperature permeability parameters by following the same procedures described in previous works.[36−38] The permeability of all batches was evaluated in a laboratory-made apparatus, with tests performed in a steady-state regime with dry airflow at room conditions (T_o = 25−29 °C, $P_o = P_{atm}$ ≈ 94.9 kPa) on two specimens from the same batch. The pressure drop across the specimen ($P_i - P_o$) was measured with a digital micromanometer (0−1000 Pa, Dwyer Mark III, series 475, Michigan, USA) in response to variations in the air volumetric flow rate Q, controlled by a needle valve, and measured with rotameters (0−400 and 300−3000 L/h, Conaut, São Paulo, Brazil). The investigated parameters were retrieved from experimental data and fitting of Forchheimer's equation (eq S(1)), an empirical relationship well accepted in the literature to express the parabolic dependence of pressure drop (ΔP) with the resulting superficial or face velocity (v_s) of a fluid through the medium,[36−38] and the details for all permeability equations and calculations were given in the supporting information.

3. RESULTS AND DISCUSSIONS

3.1. Structural Characterizations. The FTIR spectra (all normalized) of the used PU foams templates are given in Figure 1a. The characteristic urethane peak is resolved at ~3300 cm^{-1} with N−H stretching vibration.[39] Around 2940 and 2870 cm^{-1}, C−H stretching vibration is seen.[39,40] The sharp peaks around 1730 and 1645 cm^{-1} belong to ester C═O stretching bonds in urethane.[41] Other bands can be seen at 1540 cm^{-1} for N−H bending and for C−N stretching,[42] and then at 1220 and 1070 cm^{-1} for C−O−C asymmetric and symmetric vibrations, respectively.[41]

TGA results for PU foams are illustrated in Figure 1b. The largest weight loss occurred between 250 and ~ 450 °C for all foams. The only distinction between them is the residual weight after heat treatment. Foam O1 had the lowest weight loss (94.1%) followed by O2 (98.3%) and C1 (99.8%) at 1000 °C. The effects of the impregnating solvent, i.e., acetone, on the PU foams were also followed by FTIR analysis, and the results indicated no observable change, see Figure S2a,b.

FTIR spectra of as-received chemicals and preceramic precursors cross-linked at 80 °C/7 h + RT/23 h and 220 °C/2 h are shown in Figure 2. In the spectra of cross-linked precursors, the peaks around 2165 and 900 cm^{-1} and 1260 and 770 cm^{-1} are assigned to Si−H and Si−CH_3 bond vibrations, respectively.[43] In addition, Si−O bonds result in around 1055 cm^{-1} stretching.[43] The presence of vinyl groups in TMTVS leads to a peak at 3020−3057 cm^{-1} and at 1408 cm^{-1} that are characteristic for C−H vibrations of conjugated C atoms.[44] The reduction of the Si−H and vinyl peak intensities implies a progress via hydrosilylation reactions.[34,45,46] It is clear from the reduction of such Si−H peak and from the disappearance of the vinyl bond absorptions that the addition of TMTVS and of vinyl-terminated PDMS improved the cross-linking, particularly when cross-linking is operated at a higher temperature. In this regard, it is possible to state that the cross-linking process is not completely finished for the low temperature cured samples (80 °C/7 h + RT/23 h), the effects of temperature on cross-linking was already shown by calculating the molecular weight between cross-links from the polymer viscoelastic properties.[47]

The FTIR spectra of the SiOC foams produced using PU substrates O1 and O2 are shown in Figure S3a,b. All SiOC samples show similar three peaks: First, Si−O bond which belongs to Si−O−Si deformation is at 450 cm^{-1},[48] second at ~805 cm^{-1} from Si−C and Si−O stretching,[48,49] and the third, a broad peak belonging to the Si−O stretching due to Si−O−Si vibrations around 1070 cm^{-1} of the silicon oxycarbide network.[48−50] XRD analyses (Figure S4a−c) of SiOC ceramics showed no crystalline phases, but only showed broad Bragg reflections for 2θ between 10 and 30°, related to amorphous silicates, similar to previous works.[51]

3.2. Morphological Characterizations. SEM micrographs obtained from the fracture surfaces of SiOC foams processed with 100% PHMS are given in Figure 3. The PU foams O1 and O2 have open cell structures while C1 has a partially closed cell structure, resulting in the ceramic replicas shown with low-magnification images shown in Figure 3a, d,

https://dx.doi.org/10.1021/acsapm.0c00734
ACS Appl. Polym. Mater. 2020, 2, 4118−4126

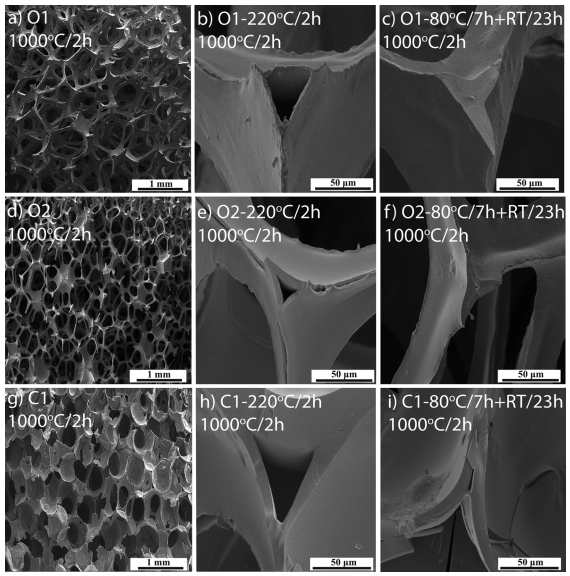

Figure 3. SEM images of SiOC ceramics made using 100% PHMS (both dense and hollow struts) obtained from PU foam types: (a–c) O1, (d–f) O2, and (g–i) C1.

and g. Cell sizes and strut thicknesses of the ceramic foams were measured as 779 ± 202 and 49.8 ± 11.2 μm (O1), 693 ± 65 and 36.3 ± 8.1 μm (O2), and 656 ± 116 and 61.5 ± 12.4 μm (C1), respectively.

It was recently shown that open-cell structured ceramic foams demonstrate improved reactivity to pressure drop trade-off when porosity was increased and strut diameter was decreased.[11] Nevertheless, the study underlined the processing limitations to form ceramic foams with strut diameters lower than 500 microns, e.g., via additive manufacturing. Here, it is demonstrated that microstructural features of SiOC ceramic foams can be deliberately tuned to obtain "dense" or "hollow" struts with less than around 60 μm thickness, see Figure 3b, c, e, f, h, and i. It is also clear that the cross-linking temperature affected the final strut morphology. As shown in Figure 3b, e, and h, the samples obtained from the curing at 220 °C/2 h had hollow struts, since the preceramic polymer blend had insufficient time to swell into the PU foam. Because of sudden curing, only the surface was coated with a film and the core became hollow after the thermal treatment and decomposition of the coated PU substrate. On the other hand, the curing conducted at 80 °C/7 h + RT/23 h gave enough time for the preceramic precursors to penetrate into the PU foam matrix and create nearly homogenous, dense strut morphology, as

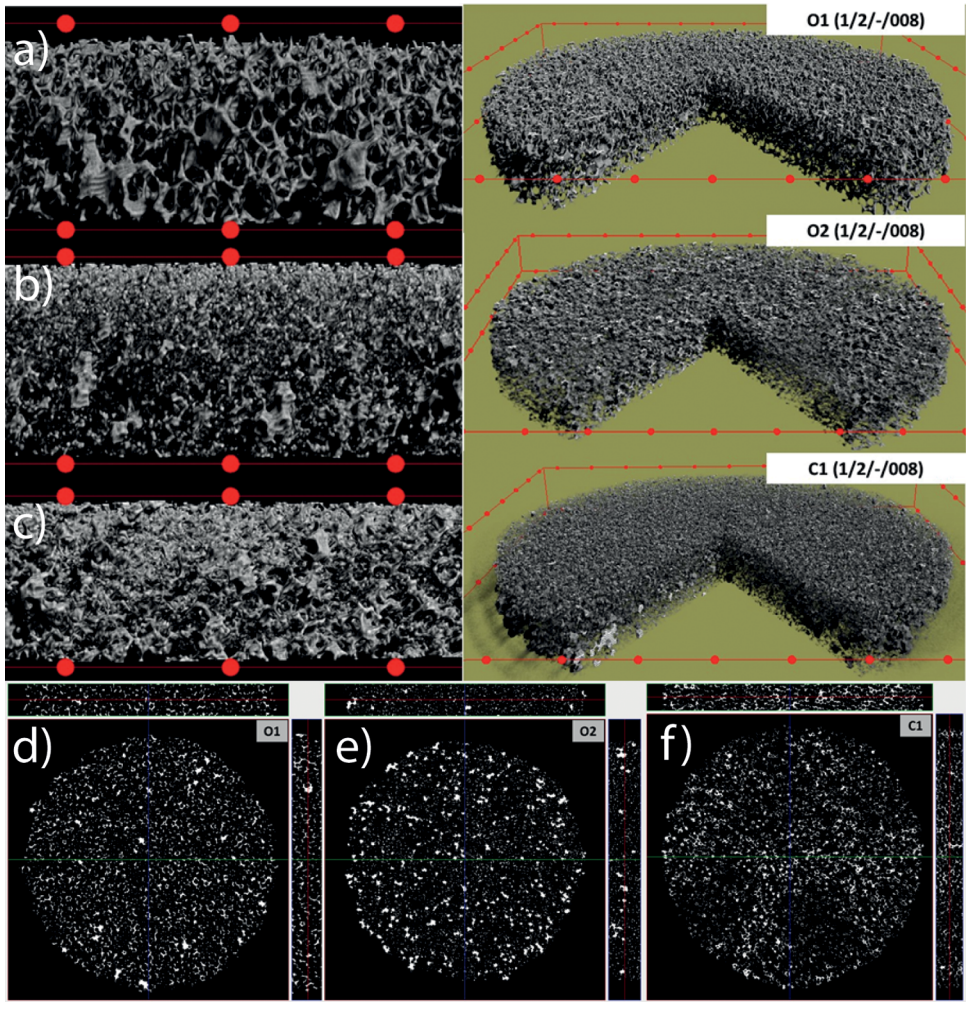

Figure 4. (a–c) 3D and (d–f) 2D tomography images of SiOC samples (100% PMHS, dense struts) obtained from O1, O2, and C1 PU foams (distance between two red points in the images is 2.5 mm).

https://dx.doi.org/10.1021/acsapm.0c00734
ACS Appl. Polym. Mater. 2020, 2, 4118–4126

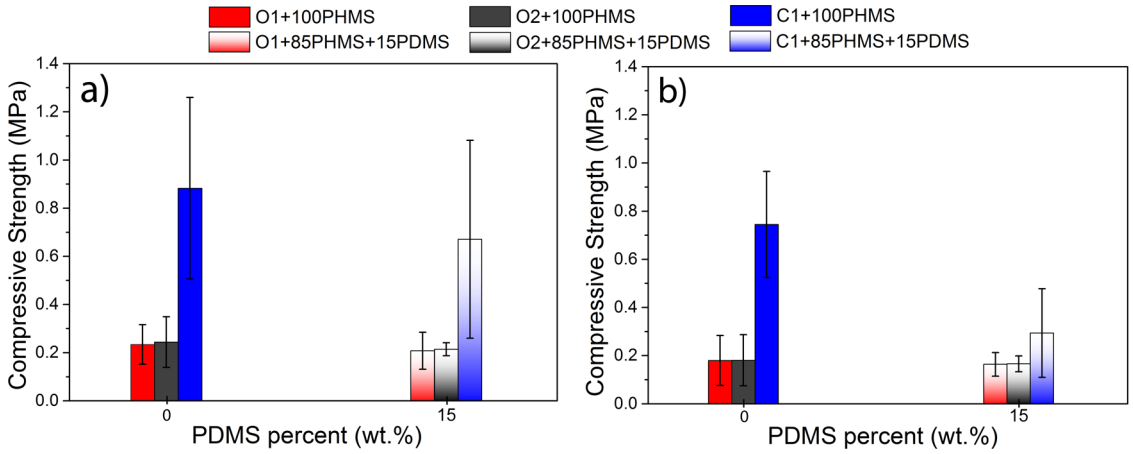

Figure 5. Compressive strength of the SiOC foams with (a) dense and (b) hollow struts.

shown in Figure 3c, f, and i. Although in these SEM images only the samples made using 100% PHMS are shown, very similar micrographs belonging to the rest of the sample set (with PDMS additions) can be seen in Figures S5–S8.

The influence of the PU substrate, preceramic precursor, and curing conditions on the skeletal density and total porosity of SiOC is shown in Figure S9. The average value found for all compositions (2226 ± 107 kg/m^3) is within the typical range reported in the literature (1964 to 2380 kg/m^3).[26,52] Such values are akin to porous carbons (1900–2400 kg/m^3), but much smaller than those for alumina (3900–4100 kg/m^3), mullite (3100–3300 kg/m^3), clay-made refractory (2500–2900 kg/m^3), and silicon carbide (3100–3200 kg/m^3). Besides this, very similar density values (2229 ± 65 kg/m^3 and 2227 ± 138 kg/m^3) were found for samples subjected to different curing conditions to yield dense or hollow struts, respectively. This implies a probable similar chemical composition for the obtained SiOC foams without any dependence on the curing condition. Besides, no conclusive influence of the PU foam on the skeletal density was verified, as can be seen in Figure S9 showing the influence of processing variables on the total porosity of SiOC foams. The average value including all compositions was 95.7 ± 2.1%, clearly increasing the PDMS in each foam type caused a further increase in the total porosity. The bodies with the lowest porosity were clearly those produced with the C1, with partially closed cells (93.5 ± 1.2% for dense and 92.8 ± 2.2% for hollow SiOC struts).

N_2 sorption analysis isotherms together with the pore size distribution were reported in Figure S10a,b showing hierarchical pores from 2 to 10 nm (peaking around 4 nm). It has been already shown that when preceramic polymer mixtures including similar PDMS components are pyrolyzed, the decomposition of such material results in the formation of 5–20 nm ranged pores and enhances the SSA.[34] This is consistent with the current observations that when no PDMS was used in the preceramic mixture, foams with very low SSA (around 1 m^2/g) were obtained, and instead when 50 wt % PDMS made foams were tested, SSA of 79.21 m^2/g was observed.

The 3D images obtained by microtomography are shown in Figure 4a–c. The previously measured porosities for the tested foams were 97.2% (O1), 96.4% (O2), and 93.2% (C1). Some macroscopic aspects were confirmed by comparison of images: (i) the O1 foam yielded a relatively homogeneous reticulated structure with larger fully interconnected and nonaligned cells; (ii) a similar pattern was observed for the O2 foam, however, with smaller cells, thinner struts and some regions of non-uniform coating; (iii) despite the lowest porosity, the C1 foam had dense solid matrix with alternated regions of poor coating which was probably due to the difficulty to swell partially closed cells. The variation in the strut coating uniformity for the C1 foam is confirmed in the 2D tomographic images in Figure 4d–f, with the presence of darker regions in the radial slices (see Figure 4f). No consistent statistical analysis was possible in the 2D images to determine the porosity and the cell size distribution, due to the high degree of 3D interconnections of struts and cells and the interference caused by the superposition of solid and void fractions among the adjacent slices.

3.3. Mechanical Properties. The effect of porosity on the cold crush strength (CCS) was comprehensively discussed in recent reviews showing that the materials with closed porosity have enhanced strength compared to those with open porosity.[13] Certainly, both relative density and the cell size affect the crushing strength: the increase in the relative density causes an increase in the strength, while, for the same relative density, the CCS decreases with the increase in pore size.[53] Analogous outcomes were achieved for the produced SiOC foams in this work; first, while there was a slight difference in the relative density values, open-cell SiOC foams (0.208–0.244 MPa) had lower crushing strength compared to those with partially closed porosity (~0.883 MPa). Example stress–strain curves obtained from the SiOC foams made using 100% PHMS for both hollow and dense struts can be seen in Figure S11. While the onset of brittle crushing was around 5% for open porous O1 and O2 which is a typical value for brittle foams,[54] for partially closed cell foams around 9% strain was observed (note that samples with dense struts had higher values compared with that of the samples having hollow struts). Besides, when the data from all samples are analyzed, it is clear that the decrease in the pore size results in an increase in the strength. Moreover, it is shown that the foams with dense struts have higher crushing strength compared to that of the ones (i) having hollow struts, as seen in Figure 5a, b and Table S1, and (ii) with 15% PDMS having hierarchical porosity in the struts (and also in their matrix). It is also important to note that the CCS values obtained from open-cell SiOC foams produced in this study are lower compared to what already observed for other open-porous SiOC components.[29] This is probably due to the combination of several

https://dx.doi.org/10.1021/acsapm.0c00734
ACS Appl. Polym. Mater. 2020, 2, 4118–4126

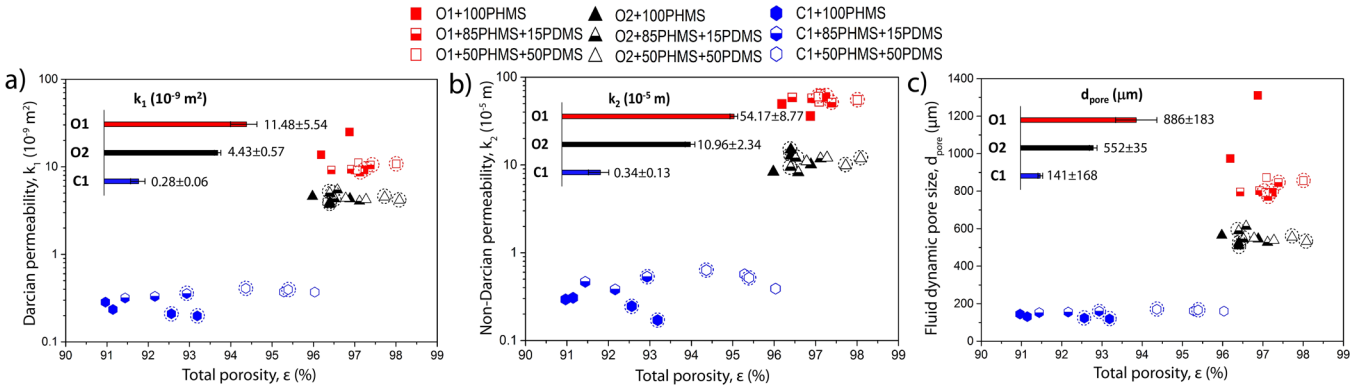

Figure 6. Fluid dynamic parameters obtained from the RT airflow permeation experiments: (a) Darcian permeability coefficient; (b) non-Darcian permeability coefficient; (c) fluid dynamic pore size. The circles surrounding the data demonstrate the foams having dense struts instead the regular data points show the ones with hollow struts.

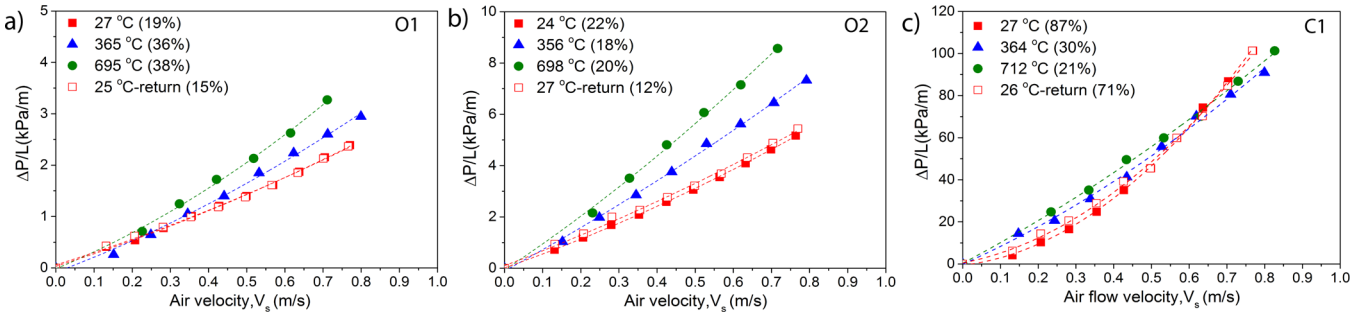

Figure 7. Permeation curves at increasing airflow temperatures for SiOC samples (85% PHMS+15% PDMS, dense struts) obtained from the PU foams type: (a) O1, (b) O2, and (c) C1.

factors such as defects formed during sample preparation (see the large scattering in the values), differences in the relative density and the cell size, the presence of residual strut porosity, and so on.

3.4. Permeability Measurements. The ranges of superficial air velocities (v_s) achieved in the ambient condition tests were 0−0.75 m/s for O1, 0−0.23 m/s for O2, and 0−0.10 m/s for C1. Despite the apparent low v_s values, the maximum contribution of inertia on total pressure drop calculated by eqs S(5) and S(6) reached in fact 37−75% (O1), 25−47% (O2), and 26−39% (C1), as given in the legend of Figure 6. This indicates that the dependence of pressure drop with v_s was not linear and that Darcy's law should not be used for fitting purposes. Indeed, the Darcian (k_1) and non-Darcian (k_2) permeability coefficients were retrieved from high-quality parabolic fittings of Forchheimer's equation (eq S(1)) and are given in Figure 6a, b as a function of the total porosity of samples. The permeability level varied more than one order of the magnitude for k_1 (0.28×10^{-9}-11.48×10^{-9} m^2) and two orders for k_2 (0.34×10^{-5}-54.17×10^{-5} m) according to the PU substrate used to produce the SiOC foams. The highest permeability was achieved for the O1 foams with larger cells, followed by the O2 foams and finally the C1 foam with partially closed cells.

The occurrence of dense or hollow struts did not affect the permeability coefficients, since the airflow through foams is essentially macroscopic around the struts and not inside them. In fact, the literature has already identified some of the main variables that affect the macroscopic flow through ceramic replicas: cell and/or window sizes, porosity, and interconnectivity among cells.[12,36] Equation S(5) was adapted from Ergun's equations to estimate the Darcian permeability coefficient (k_1) based on the knowledge of the pore size (d_{pore}) of the medium and its interconnected porosity (ε).[36] Actually, this equation is useful to estimate an effective fluid dynamic pore size once k_1 and ε of the structure are experimentally acquired. Figure 6c gives the results for d_{pore} plotted as a function of the SiOC foam porosity. Average calculated values were 886 ± 183, 552 ± 35, and 141 ± 16 μm, respectively, for O1, O2, and C1. This trend is in rough accordance with the ranges of cell size estimated from SEM images (779 ± 202, 693 ± 65, and 656 ± 116 μm). The greater discrepancy observed for the C1 samples can be explained by the lower porosity level and the presence of partially closed cell walls, implying the lowest number of open pores effective for flow and eventually affects the calculation of the fluid dynamic pore size.

The SiOC foams produced in this work are compared to other porous structures in the permeability map adapted from Innocentini et al.,[26,36−38,55−57] as shown in Figure S12. The map is made using experimental k_1 and k_2 data extracted from the literature and used to define the permeability of porous materials. The data obtained in this study shown in the graph indicate that the manipulation of the PU substrate yielded SiOC foams with permeability in a broad range of permeability, covered in the ceramic replica group. It is also worth noting the little dispersion of $k_1 \times k_2$ data in the map for samples in each foam type, regardless of the variation of these coefficients with the pore size or porosity as observed in Figure 6.

Hot gas permeability measurements were conducted only on the selected samples made using 85% PHMS+15% PDMS with

https://dx.doi.org/10.1021/acsapm.0c00734
ACS Appl. Polym. Mater. 2020, 2, 4118−4126

dense struts since these samples had the best permeability, surface area, and compressive strength combination. Such samples were evaluated for airflow permeation at three temperature levels: ≈ 25, ≈ 350, and ≈ 700 °C. Figure 7 shows the length-normalized pressure drop curves ($\Delta P/L$) for the samples tested in the three temperature levels. As expected, eq S(1) was reliably fitted ($R^2 > 0.99$) to all experimental curves, confirming the significant contribution of the inertial-quadratic term $[\rho v_s^2/k_2]$ on the pressure drop. The lowest $\Delta P/L$ level was achieved for the O1 foams with larger open cells, followed by the O2 foams and finally the C1 foam with partially closed cells, corroborating the previous trends with tests at RT.

The airflow temperature also affected the permeation profile. In the tested interval of 25−700 °C, a reduction of 69% in air density (from 1.11 to 0.34 kg/m^3) and an increase of ∼127% in air viscosity (from 1.86 × 10^{-5} to 4.22 × 10^{-5} Pa.s) are predicted from eqs S(8) and S(9). Thus, proportional changes are respectively expected in the quadratic-inertial $[\rho v_s^2/k_2]$ and in the linear-viscous $[\mu v_s/k_1]$ terms of eq S(1). Considering the rising of pressure drop levels from 25 to 700 °C as observed in Figure 7, the dominant effect was in fact the increase in the gas viscosity.

The airflow permeation tests up to 700 °C might cause irreversible (oxidation) and/or reversible (thermal expansion effects) changes in the flow paths, which could affect both the pressure drop profile and the permeability coefficients k_1 and k_2. Nevertheless, the hypothesis of irreversible modification of the microstructure with damage of struts by oxidation was disregarded, since permeation curves at RT before and after heating remained the same (see red curves in Figure 7). On the other hand, Figure S13 shows the changes in the permeability coefficients k_1 and k_2 caused by thermal expansion during the temperature increase.

The trends and ranges which can be seen from Figure S13 are in accordance with the values previously discussed for the tests conducted at RT only. Besides, foams O1 and O2 presented slight increases of k_1 and decreases of k_2 with the rise of temperature to 700 °C. Similar trends were observed for freeze cast foams,[55] for gelcasting foams,[56] for porous lanthanum carbide discs,[58] and for SiC granular filters.[38,57] Despite this, no conclusive explanation for this behavior has been proposed so far. On the other hand, the C1 foam presented opposite trends, which could be related to the thermal expansion effects in the partially closed cells.

4. CONCLUSIONS

Polymer derived silicon oxycarbide reticulated foams were produced starting from commercial polyurethane (PU) foams by the replica technique. It was demonstrated that the microstructural features of these ceramic foams can be tuned by adjusting processing parameters such as the type of the PU foam (cell size and open/partially closed cells), cross-linking parameters (temperature and time), and the nature of the cross-linking polymeric blend. With the proposed technique, it was possible to obtain a ceramic replica even with closed cells, which could not be obtained with other conventional methods. Besides, it was shown that the foam struts could be deliberately processed as "dense" or "hollow" just by altering the cross-linking conditions. At a higher temperature (220 °C), curing occurred quickly and did not allow the preceramic solution to swell the PU matrix. Accordingly, the PU struts which were just coated with the siloxane precursor decomposed and left behind an empty space during pyrolysis. On the contrary, when cross-linking was performed at a lower temperature (80 °C + RT), it occurred sluggishly, giving the precursor enough time to swell the PU matrix, resulting in dense struts. Moreover, hierarchical porosity was able to be introduced in the SiOC structure using a vinyl-terminated PDMS which decomposed and left behind a fine porosity with a corresponding increase of specific surface area reaching around 79 m^2.g^{-1} upon pyrolysis. The average porosity including all compositions was 95.7 ± 2.1%, and the highest compressive strength was around ∼0.9 MPa. Permeability measurements performed at RT indicated a variation of more than one order of the magnitude for k_1 (0.28 × 10^{-9}−11.48 × 10^{-9} m^2) and two orders for k_2 (0.34 × 10^{-5}−54.17 × 10^{-5} m) according to the PU substrate used to produce the SiOC foams. Hot air permeation tests (up to 700 °C) demonstrated the suitability of these foams for use in harsh, oxidative conditions. It can be envisaged that these foams with hierarchical porosity can be utilized as a substrate to design reusable air filtration devices for pollutants (viruses, bacteria, dust, etc.), catalytic supports, and porous components for reactions occurring in aggressive environments.

■ ASSOCIATED CONTENT

Supporting Information

The Supporting Information is available free of charge at https://pubs.acs.org/doi/10.1021/acsapm.0c00734.

Details for fluid dynamics characterization; FTIR spectra of the PU foams with acetone; structural (FTIR, XRD), morphological (SEM, density, N_2 sorption analysis), mechanical (stress−strain curves), and permeability (influence of airflow temperature on the Darcian and non-Darcian permeability coefficients) properties of the SiOC ceramic foams, and applications map for porous ceramics including the present SiOC foams (PDF)

■ AUTHOR INFORMATION

Corresponding Author

Cekdar Vakifahmetoglu − *Department of Materials Science and Engineering, Izmir Institute of Technology, Izmir 35430, Turkey*; orcid.org/0000-0003-1222-4362; Email: cekdarvakifahmetoglu@iyte.edu.tr, cvahmetoglu@gmail.com

Authors

Tugce Semerci − *Department of Materials Science and Engineering, Izmir Institute of Technology, Izmir 35430, Turkey*

Murilo Daniel de Mello Innocentini − *Course of Chemical Engineering, University of Ribeirão Preto (UNAERP), 14096-900 Ribeirão Preto, São Paulo, Brazil*

Gabriel Antonio Marsola − *Course of Chemical Engineering, University of Ribeirão Preto (UNAERP), 14096-900 Ribeirão Preto, São Paulo, Brazil*

Paulo Renato Orlandi Lasso − *Embrapa Agricultural Instrumentation, 13560-970 São Carlos, São Paulo, Brazil*

Gian Domenico Soraru − *Dipartimento di Ingegneria Industriale, Università di Trento, 38123 Trento, Italy*

Complete contact information is available at: https://pubs.acs.org/10.1021/acsapm.0c00734

Notes

The authors declare no competing financial interest.

https://dx.doi.org/10.1021/acsapm.0c00734
ACS Appl. Polym. Mater. 2020, 2, 4118−4126

■ ACKNOWLEDGMENTS

C.V.A. acknowledges the support of the Alexander von Humboldt (AvH) Foundation. M.D.M.I. would like to thank the Brazilian Agency CNPq (Process 307259/2018-8) and Ms. Isli Samara Flauzino for the help in the permeation experiments at UNAERP. G.D.S. acknowledges the support from the Italian Ministry of University and Research (MIUR) within the Programs PRIN2017-2017PMR932 "Nanostructured Porous Ceramics for Environmental and Energy Applications."

■ REFERENCES

(1) Vakifahmetoglu, C.; Pippel, E.; Woltersdorf, J.; Colombo, P. Growth of one-dimensional nanostructures in porous polymer-derived ceramics by catalyst-assisted pyrolysis. Part I: iron catalyst. *J. Am. Ceram Soc.* **2010**, *93*, 959−968.

(2) Kim, Y. W.; Jin, Y. J.; Eom, J. H.; Song, I. H.; Kim, H. D. Engineering porosity in silicon carbide ceramics. *J. Mater. Sci.* **2010**, *45*, 2808−2815.

(3) Vakifahmetoglu, C.; Buldu, M.; Karakuscu, A.; Ponzoni, A.; Assefa, D.; Soraru, G. D. High surface area carbonous components from emulsion derived SiOC and their gas sensing behavior. *J. Eur. Ceram. Soc.* **2015**, *35*, 4447−4452.

(4) Carvalho, A. C.; Raupp-Pereira, F.; Rodrigues Neto, J. B. A. P. A new source for production of ceramic filters. *Mater. Lett.* **2015**, *145*, 250−252.

(5) Zeydanli, D.; Akman, S.; Vakifahmetoglu, C. Polymer-derived ceramic adsorbent for pollutant removal from water. *J. Am. Ceram. Soc.* **2018**, *101*, 2258−2265.

(6) Zhang, F. Z.; Kato, T.; Fuji, M.; Takahashi, M. Gelcasting fabrication of porous ceramics using a continuous process. *J. Eur. Ceram. Soc.* **2006**, *26*, 667−671.

(7) Wei, Z.; Li, S.; Li, Y.; Li, X.; Xiang, R.; Xu, N. Porous alumina ceramics with enhanced mechanical and thermal insulation properties based on sol-treated rice husk. *Ceram. Int.* **2018**, *44*, 22616−22621.

(8) Shimizu, T.; Matsuura, K.; Furue, H.; Matsuzak, K. Thermal conductivity of high porosity alumina refractory bricks made by a slurry gelation and foaming method. *J. Eur. Ceram. Soc.* **2013**, *33*, 3429−3435.

(9) Medri, V.; Mazzocchi, M.; Bellosi, A. ZrB2-based sponges and lightweight devices. *Int. J. Appl. Ceram. Technol.* **2011**, *8*, 815−823.

(10) Vakifahmetoglu, C. Zeolite decorated highly porous acicular calcium silicate ceramics. *Ceram. Int.* **2014**, *40*, 11925−11932.

(11) Papetti, V.; Dimopoulos Eggenschwiler, P.; Della Torre, A.; Lucci, F.; Ortona, A.; Montenegro, G. Additive manufactured open cell polyhedral structures as substrates for automotive catalysts. *Int. J. Heat Mass Transfer* **2018**, *126*, 1035−1047.

(12) Innocentini, M. D. M.; Rodrigues, V. P.; Romano, R. C. O.; Pileggi, R. G.; Silva, G. M. C.; Coury, J. R. Permeability optimization and performance evaluation of hot aerosol filters made using foam incorporated alumina suspension. *J. Hazard. Mater.* **2009**, *162*, 212−221.

(13) Vakifahmetoglu, C.; Semerci, T.; Soraru, G. D. Closed porosity ceramics and glasses. *J. Am. Ceram. Soc.* **2020**, *103*, 2941−2969.

(14) Colombo, P.; Vakifahmetoglu, C.; Costacurta, S. Fabrication of ceramic components with hierarchical porosity. *J. Mater. Sci.* **2010**, *45*, 5425−5455.

(15) Stabler, C.; Ionescu, E.; Graczyk-Zajac, M.; Gonzalo-Juan, I.; Riedel, R. Silicon oxycarbide glasses and glass-ceramics: "All-Rounder" materials for advanced structural and functional applications. *J. Am. Ceram. Soc.* **2018**, *101*, 4817−4856.

(16) Vakifahmetoglu, C.; Colombo, P.; Carturan, S. M.; Pippel, E.; Woltersdorf, J. Growth of one-dimensional nanostructures in porous polymer-derived ceramics by catalyst-assisted pyrolysis. Part II: cobalt catalyst. *J. Am. Ceram. Soc.* **2010**, *93*, 3709−3719.

(17) Adam, M.; Vakifahmetoglu, C.; Colombo, P.; Wilhelm, M.; Grathwohl, G. Polysiloxane-derived ceramics containing nanowires with catalytically active tips. *J. Am. Ceram. Soc.* **2014**, *97*, 959−966.

(18) Lale, A.; Schmidt, M.; Mallmann, M. D.; Bezerra, A. V. A.; Acosta, E. D.; Machado, R. A. F.; Demirci, U. B.; Bernard, S. Polymer-derived ceramics with engineered mesoporosity: From design to application in catalysis. *Surf. Coat. Technol.* **2018**, *350*, 569−586.

(19) Santhosh, B.; Vakifahmetoglu, C.; Ionescu, E.; Reitz, A.; Albert, B.; Sorarù, G. D. Processing and thermal characterization of polymer derived SiCN(O) and SiOC reticulated foams. *Ceram. Int.* **2020**, *46*, 5594−5601.

(20) Kong, J.; Wang, M.; Zou, J.; An, L. Soluble and meltable hyperbranched polyborosilazanes toward high-temperature stable SiBCN ceramics. *ACS Appl. Mater. Interfaces* **2015**, *7*, 6733−6744.

(21) Patil, N.; Zhao, X.; Mishra, N. K.; Saed, M. A.; Radovic, M.; Green, M. J. Rapid heating of silicon carbide fibers under radio frequency fields and application in curing preceramic polymer composites. *ACS Appl. Mater. Interfaces* **2019**, *11*, 46132−46139.

(22) Duong, B.; Gangopadhyay, P.; Brent, J.; Seraphin, S.; Loutfy, R. O.; Peyghambarian, N.; Thomas, J. Printed sub-100 nm polymer-derived ceramic structures. *ACS Appl. Mater. Interfaces* **2013**, *5*, 3894−3899.

(23) Duong-Viet, C.; Ba, H.; El-Berrichi, Z.; Nhut, J.-M.; Ledoux, M. J.; Liu, Y.; Pham-Huu, C. Silicon carbide foam as a porous support platform for catalytic applications. *New J. Chem.* **2016**, *40*, 4285−4299.

(24) Patcas, F. C.; Garrido, G. I.; Kraushaar-Czarnetzki, B. CO oxidation over structured carriers: A comparison of ceramic foams, honeycombs and beads. *Chem. Eng. Sci.* **2007**, *62*, 3984−3990.

(25) Santoliquido, O.; Bianchi, G.; Dimopoulos Eggenschwiler, P.; Ortona, A. Additive manufacturing of periodic ceramic substrates for automotive catalyst supports. *Int. J. Appl. Ceram. Technol.* **2017**, *14*, 1164−1173.

(26) Vakifahmetoglu, C.; Zeydanli, D.; Innocentini, M. D. M.; Ribeiro, F. D. S.; Lasso, P. R. O.; Soraru, G. D. Gradient-hierarchic-aligned porosity SiOC ceramics. *Sci. Rep.* **2017**, *7*, 41049.

(27) Vakifahmetoglu, C.; Zeydanli, D.; Ozalp, V. C.; Borsa, B. A.; Soraru, G. D. Hierarchically porous polymer derived ceramics: A promising platform for multidrug delivery systems. *Mater. & Des.* **2018**, *140*, 37−44.

(28) Hammel, E. C.; Ighodaro, O. L. R.; Okoli, O. I. Processing and properties of advanced porous ceramics: An application based review. *Ceram. Int.* **2014**, *40*, 15351−15370.

(29) Choudhary, A.; Pratihar, S. K.; Agrawal, A. K.; Behera, S. K. Macroporous SiOC ceramics with dense struts by positive sponge replication technique. *Adv. Eng. Mater.* **2018**, *20*, 1700586.

(30) Soraru, G. D.; Campostrini, R.; Ejigu, A. A.; Zera, E.; Jana, P. Processing and characterization of polymer derived SiOC foam with hierarchical porosity by HF etching. *J. Ceram. Soc. Jpn.* **2016**, *124*, 1023−1029.

(31) Schelm, K.; Abreu Morales, E.; Scheffler, M. Mechanical and surface-chemical properties of polymer derived ceramic replica foams. *Materials* **2019**, *12*, 1870.

(32) Jana, P.; Zera, E.; Sorarù, G. D. Processing of preceramic polymer to low density silicon carbide foam. *Mater. & Des.* **2017**, *116*, 278−286.

(33) Jana, P.; Bruzzoniti, M. C.; Appendini, M.; Rivoira, L.; Del Bubba, M.; Rossini, D.; Ciofi, L.; Sorarù, G. D. Processing of polymer-derived silicon carbide foams and their adsorption capacity for non-steroidal anti-inflammatory drugs. *Ceram. Int.* **2016**, *42*, 18937−18943.

(34) Blum, Y.; Sorarù, G. D.; Ramaswamy, A. P.; Hui, D.; Carturan, S. M. Controlled mesoporosity in SiOC via chemically bonded polymeric "Spacers". *J. Am. Ceram. Soc.* **2013**, *96*, 2785−2792.

(35) ASTM D 3576. Standard test method for cell size of rigid cellular plastics. In *Annual Book of ASTM Standards,* West Conshohocken, PA, 1997.

(36) Innocentini, M. D. M.; Sepulveda, P.; Ortega, F. S. Permeability. In *Cellular Ceramics: Structure, Manufacture, Properties*

https://dx.doi.org/10.1021/acsapm.0c00734
ACS Appl. Polym. Mater. 2020, 2, 4118−4126

and Applications; Scheffler, M.; Colombo, P.; Wiley-VCH: Weinheim, Germany, 2005; 313−341.
(37) Innocentini, M. D. M.; Tanabe, E. H.; Aguiar, M. L.; Coury, J. R. Filtration of gases at high pressures: Permeation behavior of fiber-based media used for natural gas cleaning. *Chem. Eng. Sci.* **2012**, *74*, 38−48.
(38) Dey, A.; Kayal, N.; Chakrabarti, O.; Caldato, R. F.; Innocentini, M. D. M.; Guerra, V. G. Investigations on material and mechanical properties, air-permeation behavior and filtration performance of mullite-bonded porous SiC ceramics. *Int. J. Appl. Ceram. Technol.* **2014**, *11*, 804−816.
(39) Gabriel, L. P.; Rodrigues, A. A.; Macedo, M.; Jardini, A. L.; Maciel Filho, R. Electrospun polyurethane membranes for Tissue Engineering applications. *Mater. Sci. Eng. C* **2017**, *72*, 113−117.
(40) Adnan, S.; Tuan Ismail, T. N. M.; Mohd Noor, N.; Nek, M. D. N. S. M.; Hanzah, N.; Shoot Kian, Y.; Abu, H. H. Development of flexible polyurethane nanostructured biocomposite foams derived from palm olein-based polyol. *Adv. Mater. Sci. Eng* **2016**, *2016*, 12.
(41) Gómez-Fernández, S.; Ugarte, L.; Peña-Rodriguez, C.; Zubitur, M.; Corcuera, M. Á.; Eceiza, A. Flexible polyurethane foam nanocomposites with modified layered double hydroxides. *Appl. Clay Sci.* **2016**, *123*, 109−120.
(42) Radice, S.; Turri, S.; Scicchitano, M. Fourier transform infrared studies on deblocking and crosslinking mechanisms of some fluorine containing monocomponent polyurethanes. *Appl. Spectrosc.* **2004**, *58*, 535−542.
(43) Assefa, D.; Zera, E.; Campostrini, R.; Soraru, G. D.; Vakifahmetoglu, C. Polymer-derived SiOC aerogel with hierarchical porosity through HF etching. *Ceram. Int.* **2016**, *42*, 11805−11809.
(44) Taheri, P.; Bokka, A.; Asgari, P.; Jeon, J.; Lang, J. C.; Campostrini, R.; Sorarù, G. D.; Kroll, P. Novel sulfur-containing cross-linking agent for Si-based preceramic polymers. *Macromol. Chem. Phys.* **2020**, *221*, 1900380.
(45) Sorarù, G. D.; Dalcanale, F.; Campostrini, R.; Gaston, A.; Blum, Y.; Carturan, S.; Aravind, P. R. Novel polysiloxane and polycarbosilane aerogels via hydrosilylation of preceramic polymers. *J. Mater. Chem.* **2012**, *22*, 7676−7680.
(46) Marciniec, B. Functionalisation and cross-linking of organosilicon polymers. In *Hydrosilylation: A Comprehensive Review on Recent Advances*; Marciniec, B; Springer: Netherlands, 2009, pp. 159−189.
(47) Lau, T. H. M.; Wong, L. L. C.; Lee, K.-Y.; Bismarck, A. Tailored for simplicity: creating high porosity, high performance bio-based macroporous polymers from foam templates. *Green Chem.* **2014**, *16*, 1931−1940.
(48) Ishihara, S.; Nishimura, T.; Tanaka, H. Precipitation processing to synthesize fine polycarbosilane particles for precursors of silicon carbide powders. *J. Ceram. Soc. Jpn.* **2006**, *114*, 507−510.
(49) Liu, X.; Li, Y.-L.; Hou, F. Fabrication of SiOC ceramic microparts and patterned structures from polysiloxanes via liquid cast and pyrolysis. *J. Am. Ceram. Soc.* **2009**, *92*, 49−53.
(50) Narisawa, M.; Funabiki, F.; Iwase, A.; Wakai, F.; Hosono, H. Effects of atmospheric composition on the molecular structure of synthesized silicon oxycarbides. *J. Am. Ceram. Soc.* **2015**, *98*, 3373−3380.
(51) Vakifahmetoglu, C.; Balliana, M.; Colombo, P. Ceramic foams and micro-beads from emulsions of a preceramic polymer. *J. Eur. Ceram. Soc.* **2011**, *31*, 1481−1490.
(52) Stabler, C.; Reitz, A.; Stein, P.; Albert, B.; Riedel, R.; Ionescu, E. Thermal properties of SiOC glasses and glass ceramics at elevated temperatures. *Materials (Basel)* **2018**, *11*, 279.
(53) Colombo, P.; Bernardo, E.; Biasetto, L. Novel microcellular ceramics from a silicone resin. *J. Am. Ceram. Soc.* **2004**, *87*, 152−154.
(54) Colombo, P.; Modesti, M. Silicon Oxycarbide Ceramic Foams from a Preceramic Polymer. *J. Am. Ceram. Soc.* **1999**, *82*, 573−578.
(55) Barg, S.; Innocentini, M. D. M.; Meloni, R. V.; Chacon, W. S.; Wang, H.; Koch, D.; Grathwohl, G. Physical and high-temperature permeation features of double-layered cellular filtering membranes prepared via freeze casting of emulsified powder suspensions. *J. Membr. Sci.* **2011**, *383*, 35−43.
(56) Potoczek, M.; Chmielarz, A.; Innocentini, M. D. M.; Silva, I. C. P.; Colombo, P.; Winiarska, B. Porosity effect on microstructure, mechanical, and fluid dynamic properties of Ti2AlC by direct foaming and gel-casting. *J. Am. Ceram. Soc.* **2018**, *101*, 5346−5357.
(57) Dey, A.; Kayal, N.; Chakrabarti, O.; Innocentini, M. D. M.; Chacon, W. S.; Coury, J. R. Evaluation of air permeation behavior of porous SiC ceramics synthesized by oxidation-bonding technique. *Int. J. Appl. Ceram. Technol.* **2013**, *10*, 1023−1033.
(58) Biasetto, L.; Innocentini, M. D. M.; Chacon, W. S.; Corradetti, S.; Carturan, S.; Colombo, P.; Andrighetto, A. Gas permeability of lanthanum oxycarbide targets for the SPES project. *J. Nucl. Mater.* **2013**, *440*, 70−80.

https://dx.doi.org/10.1021/acsapm.0c00734
ACS Appl. Polym. Mater. 2020, 2, 4118−4126